Geoid
Journal of Geodesy and Geomatics

Geoid Vol. 20, No. 2, 2025, 93-113

P-ISSN: 1858-2281; E-ISSN: 2442-3998

Comparative Analysis Of Landsat 8 And Landsat 9 Sattellite Image Data In Surface Temperature Estimation, NDVI and NDBI Using Goggle Earth Engine

Dana Purwoko[*1,2], Eko Yuli Handoko[1], Ardhasena Sopaheluwakan[2]
[1]Department of Geomatics Engineering, Institut Teknologi Sepuluh Nopember, 60111, Surabaya, Indonesia
[2]Agency for Meteorology Climatology and Geophysics (BMKG), 10610, Jakarta, Indonesia
*Corresponding author: danapurwoko@gmail.com

Received: 20 August 2025; Revised: 6 November 2025; Accepted: 1 Desember 2025; Published: 10 Desember 2025

Abstract: The rapid urbanization in major cities like Jakarta significantly alters land cover, which in turn impacts environmental thermal conditions and ecological quality. This research aims to analyze the spatial and temporal dynamics of Land Surface Temperature (LST), Normalized Difference Vegetation Index (NDVI), and Normalized Difference Built-up Index (NDBI) in DKI Jakarta during the 2023–2024 period using combined data from the Landsat 8 and 9 satellites. Cross-validation analysis shows a very high level of consistency between the sensors, validating the use of combined data for multi-temporal studies. Analysis methods include land cover classification, linear regression analysis, and temporal change analysis. The results indicate a clear Urban Heat Island (UHI) phenomenon, characterized by a strong positive correlation between LST and NDBI ($R > 0.67$) and a negative correlation between LST and NDVI ($R \approx -0.5$). Temporal analysis indicates that thermal conditions in 2024 were generally lower than in 2023, and localized dynamics of land cover change were also identified. These findings affirm the fundamental relationship between land cover composition and the urban microclimate, and underscore the importance of vegetation in mitigating high temperatures in urban environment.

Keywords : Landsat; LST; NDVI; NDBI; Google Earth Engine

How to cite: Purwoko, D., Handoko, E.Y., & Sopaheluwakan, A. (2025) Comparative Analysis Of Landsat 8 And Landsat 9 Satellite Image Data In Surface Temperature Estimation, NDVI and NDBI Using Goggle Earth Engine. *Geoid, 20(2), 93-113*.

Introduction

Global climate change is a major issue impacting human life, particularly in the environmental, agricultural, and infrastructure sectors. One of its significant consequences is the rise in surface temperatures, which necessitates accurate monitoring and analysis to support adaptation and mitigation planning. The analysis of satellite imagery is a common method for obtaining Land Surface Temperature (LST) (Mashudi and Faisol, 2022). Satellite data provides information on the Earth's surface temperature with high spatial resolution and broad area coverage (Li et al., 2013; Jiménez-Muñoz et al., 2014). Furthermore, remote sensing technology, particularly Landsat satellite data, is widely applied in hydrology, meteorology, and surface energy balance studies for LST estimation (Tang et al., 2015; Meng & Cheng, 2018).

Remote sensing technology, particularly data from the Landsat satellites, offers the capability to monitor Land Surface Temperature (LST) consistently at a detailed spatial scale. Two key indicators frequently used to analyze LST are the Normalized Difference Vegetation Index (NDVI), which represents vegetation density, and built-up density, which can be estimated using indices such as the Normalized Difference Built-up Index (NDBI) (Weng et al., 2004; Zha et al., 2003). Vegetation is known to have a cooling effect through evapotranspiration, while buildings and other impervious surfaces absorb and retain heat.

The Landsat 8 and Landsat 9 satellites, part of the ongoing Landsat mission, provide critical multispectral data for environmental analysis (USGS, 2021). Each is equipped with an Operational Land Imager (OLI) and a Thermal Infrared Sensor (TIRS), enabling the estimation of Land Surface Temperature (LST) at high spatial and temporal resolutions. Landsat 9, launched in 2021, continues the data record of Landsat 8 (2013-present)

but features improved sensor sensitivity. A key enhancement is in its TIRS-2 instrument, which measures surface temperature using Bands 10 and 11 (100 m resolution) while mitigating the stray light artifacts that affected Landsat 8's TIRS data (Masek et al., 2020). Although the satellites share identical spectral band ranges, Landsat 9 has a higher radiometric resolution of 14 bits compared to Landsat 8's 12 bits. This superior resolution allows for a wider dynamic range, preventing sensor saturation over extremely bright or dark targets and capturing finer radiometric detail (Xu et al., 2024).

Google Earth Engine (GEE) provides significant advantages as a platform for satellite image analysis, primarily due to its large-scale, cloud-based processing capabilities and its extensive historical data archives (Kumar and Mutanga, 2018). The platform's data catalog hosts a vast collection of geospatial data from numerous satellites (Tamiminia et al., 2020), which is accessible via an Application Programming Interface (API) that facilitates rapid prototyping and result visualization (Gorelick et al., 2017). Consequently, GEE's cloud-based technology is widely employed for monitoring global climate and weather changes (Jannah & Bioresita, 2023). Additionally, it can be utilized for surface temperature analysis using satellite imagery available in near real-time (Prayogo, 2021).

Jakarta was selected as the study area due to its status as a megacity undergoing rapid urbanization, which has resulted in massive land cover changes. The conversion of green open spaces into dense built-up areas causes surface temperatures in urban areas to be higher than in the surrounding rural areas. The spatial dynamics between vegetation (NDVI) and built-up areas (NDBI) in Jakarta are therefore highly relevant for analyzing their correlation with the distribution of Land Surface Temperature (LST). Consequently, the accurate monitoring of LST and the analysis of its relationship with urban (NDBI) and ecological (NDVI) indicators are essential to support sustainable urban planning and spatial management policies.

This research utilizes the Google Earth Engine (GEE) platform for a comparative analysis of Land Surface Temperature (LST), Normalized Difference Vegetation Index (NDVI), and Normalized Difference Built-up Index (NDBI) in the DKI Jakarta region using imagery from Landsat 8 and Landsat 9. The analysis first evaluates the accuracy of the LST estimations by correlating them with in-situ air temperature data from multiple observation stations. Subsequently, it assesses the consistency of the LST, NDVI, and NDBI products derived from both satellites. Finally, the study identifies the correlations between LST and both NDBI and NDVI using a combined Landsat 8 and 9 dataset. This research, therefore, offers insights into the effectiveness of GEE for performing multi-sensor comparative analysis.

Data and Methods

This study focuses on the Jakarta city region, utilizing satellite imagery to derive Land Surface Temperature (LST) and correlating it with in-situ daily maximum air temperature data. The selected ground-based air temperature monitoring stations include Pantai Indah Kapuk and the Port of Tanjung Priok in North Jakarta; Kemayoran in Central Jakarta; and Halim, TMII, and Cibubur in East Jakarta. A map of the study area and the specific locations of the observation points is provided in Figure 1.

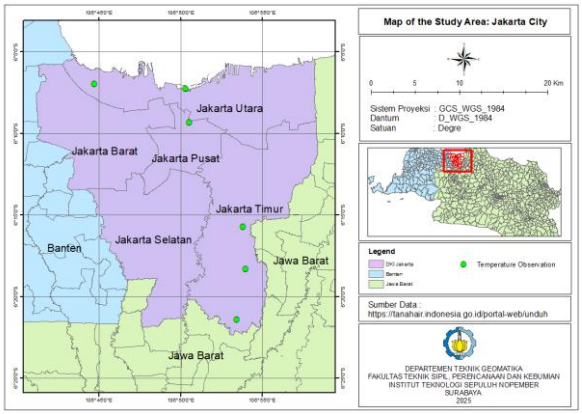

Figure 1. Map of the study area.

Landsat 8 and Landsat 9 Level-2 imagery data were obtained via Google Earth Engine. The images used were acquired on multiple dates in 2023 and 2024 with a cloud cover of less than 20%. Daily maximum air temperature data were obtained from the Indonesian Agency for Meteorology, Climatology, and Geophysics (BMKG) for dates corresponding to the satellite image acquisitions. In addition, the maximum air temperature between 10:00–11:00 AM was also recorded, which approximates the satellite's overpass time.

Land Surface Temperature (LST) was derived from the thermal band (Band 10) of the satellite imagery, where the pixel values were converted to degrees Celsius according to the standard formula (Sampelan et al., 2024).

$$LST°\text{C} = (DN * M) + A - 273.15$$

Where:

LST°C = The final Land Surface Temperature in degrees Celsius.

DN = The Digital Number or raw pixel value from the image.

M (Scale Factor) = The multiplicative scaling factor, which is 0.00341802.

A (Offset) = The additive scaling factor, which is 149.

The Normalized Difference Vegetation Index (NDVI) is used to quantify vegetation greenness and is useful for understanding vegetation density as well as assessing changes in plant health. This vegetation index is a value derived from the comparison between the reflectance values of the red and near-infrared bands. NDVI values range from -1 to +1, where high positive values (approaching +1) indicate dense and healthy vegetation, values near zero indicate non-vegetated areas such as bare soil or rock, and negative values typically represent water bodies, snow, or clouds.

For the processing in Google Earth Engine (GEE), the pixel values of Band 5 (NIR) and Band 4 (Red) were first converted to surface reflectance before the index calculation (USGS, 2025; USGS, 2024).

$$\rho = (DN * M) + A$$

Where:

ρ (Surface Reflectance) = The final, unitless surface reflectance value.

DN = The Digital Number or raw pixel value from the image.

M (Scale Factor) = The multiplicative scaling factor, which is 0.0000275.

A (Offset) = The additive scaling factor, which is -0.2.

The equation used to calculate the NDVI value is as follows (Putu Aryastana et al., 2023; Hardianto et al., 2021) :

$$\text{NDVI} = \frac{(NIR - RED)}{(NIR + RED)}$$

Where:

NIR = Reflectance value of the near-infrared band (Band 5).

RED = Reflectance value of the red band (Band 4).

Table 1. NDVI (Normalized Difference Vegetation Index) classification scheme

Table 1. NDVI value classification for vegetation density (Laksono et al., 2020)

NDVI Value	Classification
-1,00 sd 0,00	Non-Vegetated
0,00 sd 0,30	Slightly density
0,30 sd 0,60	Moderately density
0,60 sd 1,00	Highly density

The Normalized Difference Built-up Index (NDBI) is a remote sensing index used to identify and map built-up areas. This index works by utilizing the difference in spectral reflectance between the short-wave infrared (SWIR) and near-infrared (NIR) channels. Built-up areas tend to reflect more energy in the SWIR waveband compared to the NIR waveband. NDBI values range from -1 to +1, where high positive values indicate built-up areas, while negative values indicate vegetation cover or water bodies.

The NDBI processing in Google Earth Engine (GEE) involved first converting the pixel values of Band 6 (SWIR 1) and Band 5 (NIR) to surface reflectance before applying the index formula (USGS, 2025; USGS, 2024).

$$\rho = (DN * M) + A$$

Where:

ρ (Surface Reflectance) = The final, unitless surface reflectance value.

DN = The Digital Number or raw pixel value from the image.

M (Scale Factor) = The multiplicative scaling factor, which is 0.0000275.

A (Offset) = The additive scaling factor, which is -0.2.

The equation used to calculate the NDBI value is as follows (Gunawan et al., 2023):

$$NDBI = \frac{(SWIR - NIR)}{(SWIR + NIR)}$$

Where:

SWIR = Reflectance value of the short wave infrared (band 6).

NIR = Reflectance value of the near infrared (band 5).

The classification scheme for built-up land (NDBI) is presented in Table 2.

Table 2. Built-up land value classification (NDBI) (Gunawan et al., 2023)

NDBI Value	Classification
-1,0 sd 0,0	Non-Built-up Area
0,0 sd 0,1	Sparse Built-up
0,1 sd 0,2	Danse Built-up Area
0,2 sd 0,3	Very Dense Building

The entire processing workflow for LST, NDVI, and NDBI was coded in JavaScript within the Google Earth Engine code editor. The research methodology is illustrated in the flowchart in Figure 2.

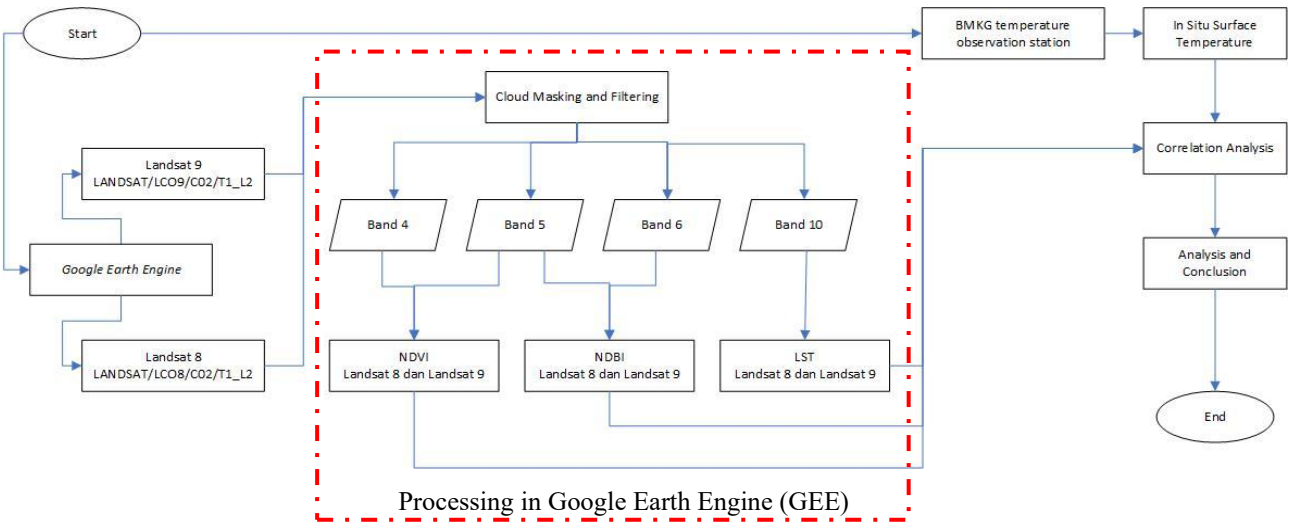

Figure 2. Flowchart of the research methodology.

Pearson correlation analysis was used to measure the strength of the linear relationship between the estimated Land Surface Temperature (LST) and the maximum air temperature, NDVI and NDBI. The Pearson correlation coefficient (R) is calculated using the following formula (Gusmiarti et al., 2022):

$$R = \frac{n\sum xy - \sum x \sum y}{\sqrt{n\sum x^2 - (\sum x)^2}\ \sqrt{n\sum y^2 - (\sum y)^2}}$$

Where :

x = Observed value.y = Predicted value.n = Total number of samples.

The strength of the linear relationship is then interpreted based on the correlation coefficient classification proposed by (Sugiyono, 2020), as shown below:

Table 3. Interpretation of the correlation coefficient

Coefficient Value	Interpretation
0,00 –0,199	Very low
0,20 –0,399	Low
0,40 –0,599	Medium
0,60 –0,799	Strong
0,80 –1,000	Very strong

Where X and Y are the estimated LST value and the measured air temperature value, while n is the total number of samples. The value of R ranges from –1 to +1, with an absolute value approaching 1 indicating a strong linear relationship.

The coefficient of determination (R^2) is calculated as the square of R (Mustafa, 2023) and represents the proportion of variance in the dependent variable (LST) that can be explained by the independent variable (air temperature). Its value ranges from 0 to 1.

$$R^2 = (R)^2 \times 100\%$$

Where :

R = Pearson's correlation coefficient.

R^2 = Coefficient of determination, representing the proportion of variance in Y predictable from X.

The accuracy of the LST estimation was measured by calculating the Root Mean Square Error (RMSE) and the Mean Absolute Error (MAE). The RMSE is calculated as the square root of the average of the squared differences between the estimated (Y_i) and observed (X_i) values, according to the formula (Fatkhuroyan & TrinahWati, 2018):

$$\text{RMSE} = \sqrt{\frac{1}{n}\sum_{i=1}^{n}(Xi - Yi)^2}$$

Where :

Xi = Observed value.

Yi = Predicted value.

n = Total number of samples.

A lower RMSE value indicates a smaller prediction error. Meanwhile, the Mean Absolute Error (MAE) is calculated as the average of the absolute differences between the estimated and observed values, as shown in the formula (Fatkhuroyan & TrinahWati, 2018) :

$$\text{MAE} = \frac{1}{n}\sum_{i=1}^{n}|Xi - Yi|$$

Where :

Xi = Observed value.

Yi = Predicted value.

n = Total number of samples.

|·| = Absolute value.

The Mean Absolute Error (MAE) measures the average prediction error in the same units as the original data and is less sensitive to extreme values.

Results and Discussion

Comparative Analysis of Landsat 8 and Landsat 9 LST with In-Situ Air Temperature

The linear regression analysis between Land Surface Temperature (LST) and in-situ air temperature revealed spatially variable results across the observation sites. On average, Landsat 8 exhibited stronger correlations than Landsat 9 (Figure 3a): the mean R-values for Landsat 8 were 0.8719 (with 10:00–11:00 AM air temperature) and 0.7757 (with daily maximum), compared to 0.7335 and 0.6543 for Landsat 9, respectively. These differences were more pronounced at specific locations. For instance, the Kemayoran station showed a much stronger correlation for Landsat 8 (R = 0.9019) than for Landsat 9 (R = 0.4456) when compared with the 10:00–11:00 AM air temperature. While the Halim and TMII stations consistently yielded strong correlations for both satellites, the Kemayoran station was characterized by weaker correlations, especially for Landsat 9. A consistent finding across all sites was that air temperature data from 10:00–11:00 AM, which is closer to the satellite overpass time, correlated more strongly with LST than the daily maximum air temperature data.

The pattern of the coefficient of determination (R^2) mirrored that of the correlation coefficient (R), with Landsat 8 generally showing higher values than Landsat 9 (Figure 3b). On average, the R^2 values for Landsat 8 were 0.7417 (with 10:00–11:00 AM temperature) and 0.7056 (with daily temperature), compared to 0.5652 and 0.4962 for Landsat 9. Despite the higher averages for Landsat 8, there was significant inter-site variability. The Halim and TMII stations, for example, consistently showed high R^2 values, indicating that air temperature is a strong predictor of LST in those areas. Conversely, the Kemayoran station exhibited low predictive power, especially for Landsat 9, where air temperature explained only a small proportion of LST variance ($R^2 = 0.1986$ with 10:00-11:00 AM data). A consistent finding for both satellites was that the 10:00–11:00 AM air temperature data explained a greater proportion of LST variance than the daily maximum temperature data.

The comparative analysis revealed that spatially, Landsat 8 generally maintained a slightly stronger linear relationship with in-situ air temperature than Landsat 9 across the study sites in Jakarta. This is reflected by the higher average R and R^2 values observed for Landsat 8 with both types of air temperature data. Additionally, the analysis confirmed that air temperature measurements closer to the satellite overpass time (10:00–11:00 AM) yield a stronger and more consistent correlation with LST than daily maximum temperatures. While estimation accuracy was found to be site-dependent, the use of daily data generally produced slightly smaller errors.

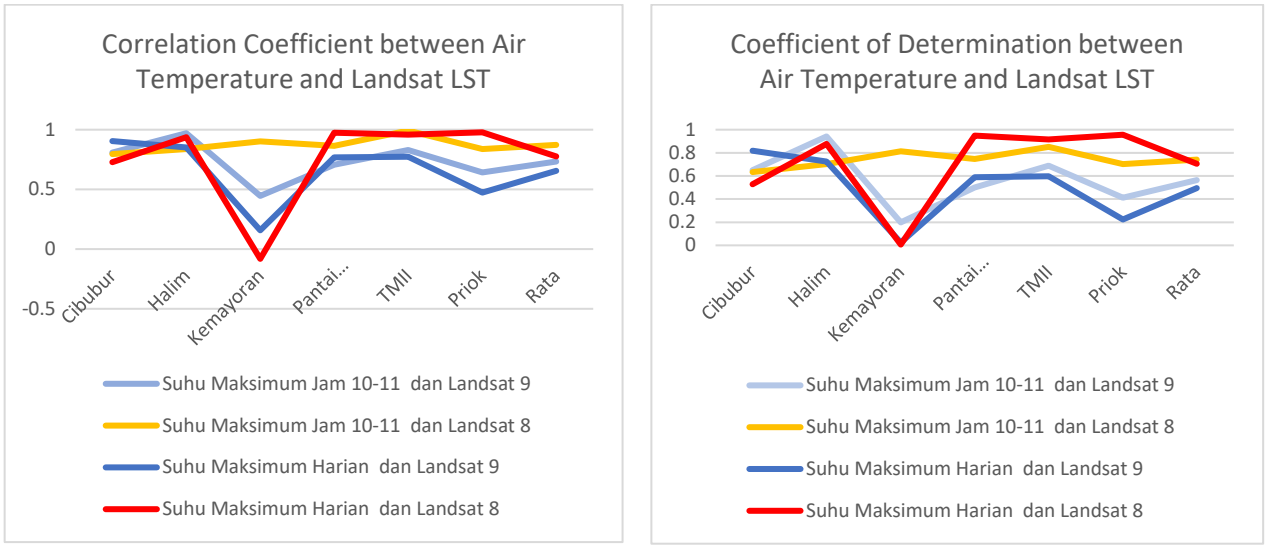

(a) (b)

Figure 3. Graphs showing (a) the correlation coefficient and (b) the coefficient of determination between in-situ air temperature and Landsat-derived LST.

A Comparative Analysis of LST, NDVI, and NDBI from Landsat 8 and Landsat 9

To ensure the reliability and continuity of the data, a consistency validation was performed on the Land Surface Temperature (LST), NDVI, and NDBI data produced by the Landsat 8 and Landsat 9 satellites. This validation was conducted through linear regression analysis using a random pixel sampling method across the entire study area. The LST, NDVI, and NDBI values from both satellites were extracted at each sample point for statistical analysis.

The validation results for the year 2023, as presented in Figure 4a, show a very high degree of consistency between the two sensors. The correlation coefficient (R) reached 0.8955, indicating a statistically very strong positive linear relationship. Furthermore, the coefficient of determination (R^2) of 0.8019 implies that approximately 80.19% of the variability in Landsat 8 LST data can be explained by the variability in Landsat 9 LST data. The resulting errors were also low, with a Root Mean Square Error (RMSE) of 1.94°C and a Mean Absolute Error (MAE) of 1.60°C, signifying high accuracy and minimal measurement discrepancies between the sensors.

For the 2024 period (Figure 4b), the LST data from both satellites remained consistent, although with a slightly lower degree of agreement compared to the previous year. The correlation coefficient (R) was recorded at 0.8687, which still indicates a strong relationship and a similar pattern. However, the R^2 value decreased to 0.7546. An increase in error was also identified, with the RMSE and MAE rising to 2.70°C and 2.32°C, respectively. Although this discrepancy is larger, the values remain within an acceptable range for comparative LST studies.

Overall, this regression analysis confirms that the LST data from Landsat 8 and Landsat 9 are reliable and consistent across both observation periods. This finding affirms that the data from both sensors are interchangeable, which is crucial for multi-temporal analysis and long-term environmental monitoring. The slight variation in consistency between the years implies that factors such as temporal atmospheric conditions may have an influence, but this does not diminish the overall validity of using the combined data from both satellites.

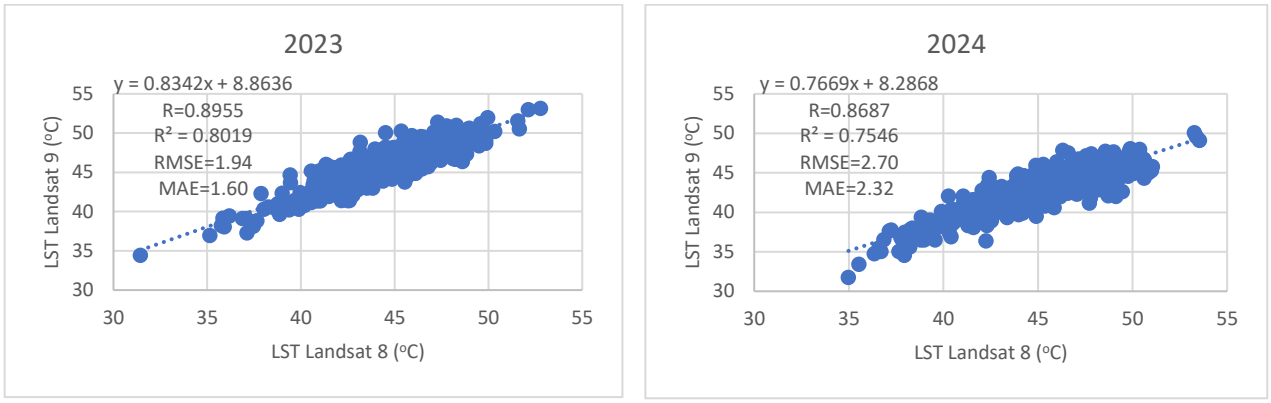

(a) (b)

Figure 4. Scatter plots comparing Land Surface Temperature (LST) from Landsat 8 and Landsat 9 for (a) 2023 and (b) 2024

Validation of the Normalized Difference Vegetation Index (NDVI) was conducted to test the degree of consistency and agreement between the sensors on the Landsat 8 and Landsat 9 satellites. This analysis is crucial to ensure that data from both missions can be combined for multi-temporal vegetation studies. The validation results from the linear regression analysis for the years 2023 and 2024 are presented in Figure 5. Overall, the findings show a very high and stable level of consistency across both observation periods.

For the year 2023 (Figure 5a), the analysis revealed a statistically very high degree of agreement. The correlation coefficient (R) reached 0.9800, indicating a near-perfect positive linear relationship between the NDVI data from both sensors. The high coefficient of determination (R^2), at 0.9603, further reinforces this finding, implying that 96.03% of the variability in Landsat 8's NDVI values can be explained by the variability in Landsat 9's NDVI. Furthermore, the resulting errors were very low, with an RMSE of 0.03 and an MAE of 0.02. Given the theoretical range of NDVI is -1 to +1, this level of error can be considered negligible and signifies nearly identical measurement accuracy.

The results for 2024 (Figure 5b) also demonstrated an exceptional level of consistency, in line with the findings from the previous year. The correlation coefficient (R) remained very high at 0.9713, with an R^2 value of 0.9434. Although there was a slight increase in error (RMSE=0.04; MAE=0.03), the difference is marginal and does not significantly reduce the degree of agreement between the sensors. This proves that the performance of both sensors in measuring vegetation greenness remained stable across both time periods.

Based on this regression analysis, it can be concluded that the NDVI data produced by Landsat 8 and Landsat 9 are statistically almost indistinguishable. The consistently high correlation ($R > 0.97$) and low MAE (≤ 0.03) provide strong evidence that the data from both satellites are interchangeable. This reliability allows for the combination of data from both missions to build denser and more robust time-series datasets for vegetation monitoring applications

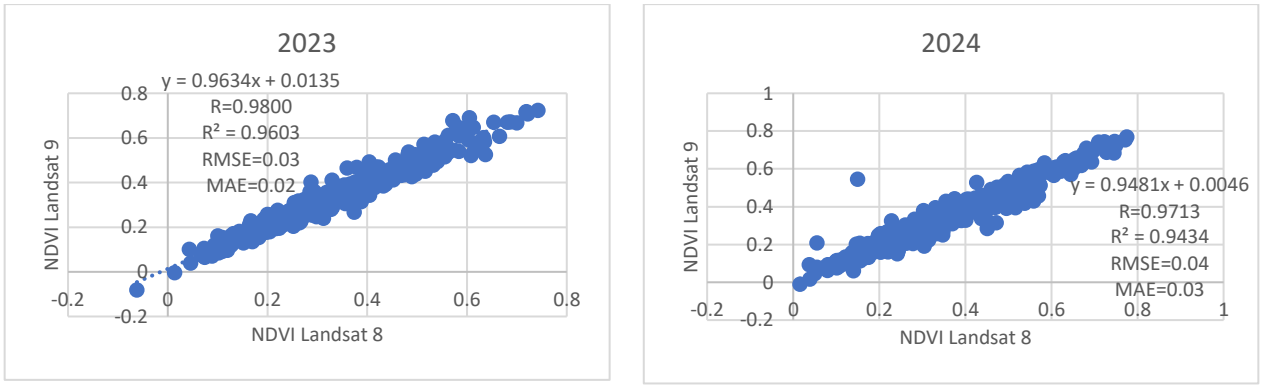

(a) (b)

Figure 5. Scatter plots comparing NDVI from Landsat 8 and Landsat 9 for (a) 2023 and (b) 2024

Validation of the Normalized Difference Built-up Index (NDBI) was conducted to evaluate the degree of consistency and agreement between the data produced by the Landsat 8 and Landsat 9 satellites. This analysis aims to ensure that both sensors provide comparable and reliable measurements of built-up areas for multi-temporal analysis. The results of the linear regression analysis for the 2023 and 2024 periods are presented in Figure 6.

For the year 2023 (Figure 6a), the analysis shows a statistically very high degree of agreement. The correlation coefficient (R) was recorded at 0.9641, which indicates a very strong positive linear relationship. The coefficient of determination (R^2) reached 0.9295, meaning 92.95% of the variability in the NDBI data from Landsat 8 can be explained by the variability in the data from Landsat 9. The resulting errors were also very low, with a Root Mean Square Error (RMSE) of 0.03 and a Mean Absolute Error (MAE) of 0.02. Given the theoretical range of NDBI is -1 to +1, this level of error can be considered practically insignificant.

The results for 2024 (Figure 6b) again showed an exceptional and even slightly stronger level of consistency. The correlation coefficient (R) increased slightly to 0.9660 with an R^2 of 0.9332. While the MAE value remained very low at 0.02, the RMSE was recorded at 0.04. These results confirm that the performance of both sensors in measuring the distribution of built-up areas was very stable and consistent across both observation periods.

Overall, it can be concluded that the NDBI data produced by Landsat 8 and Landsat 9 are highly reliable and have a very high degree of agreement. The consistently high correlation (R > 0.96) and a MAE not exceeding 0.02 in both years provide strong evidence that there are no significant systematic differences between the two sensors. Therefore, the NDBI data from both satellites can be used interchangeably, providing flexibility and reliability in studies monitoring urban dynamics.

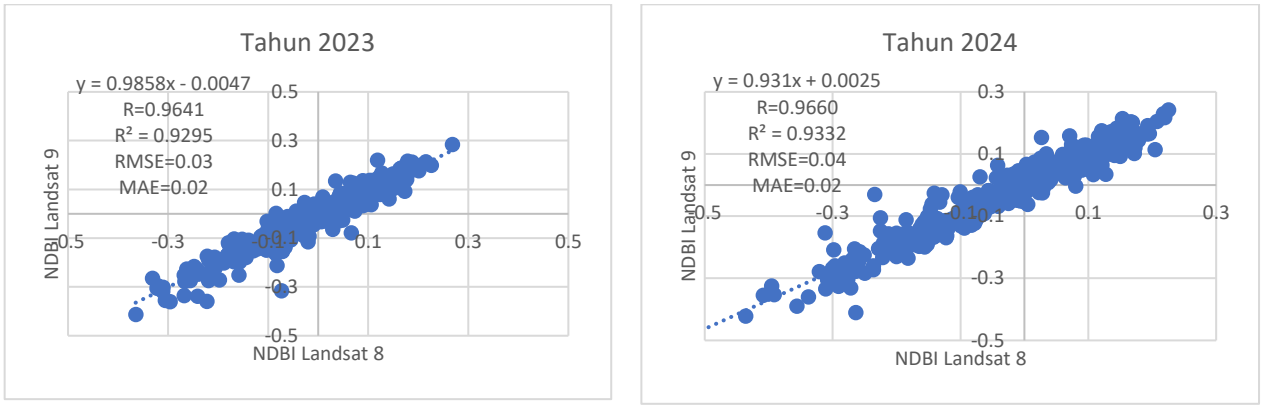

(a) (b)

Figure 6. Scatter plots comparing NDBI from Landsat 8 and Landsat 9 for (a) 2023 and (b) 2024

The cross validation analysis between the data produced by the Landsat 8 and Landsat 9 satellites convincingly demonstrates a very high degree of consistency. The highest degree of statistical agreement was exceptionally shown for the NDVI and NDBI indices. For both of these indices, consistent Pearson's correlation (R) values above 0.96 and a very low Mean Absolute Error (MAE) ($\leq$ 0.03) indicate that the data from the two satellites are statistically almost indistinguishable. At this level, the error can be considered negligible, allowing the NDVI and NDBI data from both sensors to be considered identical for most practical applications. On the other hand, although the LST data also shows a strong correlation (R > 0.86), its degree of consistency is quantitatively slightly below that of NDVI and NDBI. This is shown by a more measurable mean absolute error (MAE), ranging from 1.6°C to 2.7°C, which indicates that minor yet persistent thermal variations exist between the sensors.

The primary implication of this finding is that data from Landsat 8 and 9 can be combined and used interchangeably. The demonstrated reliability, particularly for the NDVI and NDBI indices, strongly supports the creation of denser and more accurate time-series datasets for studies on vegetation and urbanization dynamics. Meanwhile, for applications involving high-precision thermal (LST) data, users are advised to be aware of the potential for small variations that, although low, are inherent between the two sensors.

Analysis of the Relationship between LST and NDVI Using Combined Landsat 8 and Landsat 9 Data

Based on the results of the cross validation analysis between the data generated by the Landsat 8 and Landsat 9 satellites, a very high degree of consistency was shown for the three derived products Land Surface Temperature (LST), Normalized Difference Vegetation Index (NDVI), and Normalized Difference Built-up Index (NDBI) during the 2023 and 2024 observation periods. This forms the basis for combining and using data from Landsat 8 and Landsat 9, which are subsequently used to produce the LST, NDVI, and NDBI products.

To examine the quantitative relationship between surface thermal conditions and vegetation density, a linear regression analysis was performed between Land Surface Temperature (LST) and the Normalized Difference Vegetation Index (NDVI). The analysis results for the 2023 and 2024 periods are presented in Figure 7. In general, the results from both observation periods consistently show a negative correlation between LST and NDVI, which scientifically confirms that areas with higher surface temperatures tend to have lower vegetation cover.

In 2023 (Figure 7a), the analysis showed a moderate negative correlation with a correlation coefficient (R) of -0.5485. The coefficient of determination (R^2) was recorded at 0.3009, indicating that approximately 30.1% of the total variability in NDVI values within the study area can be explained by the variability in LST. The relatively clustered distribution of data points around the regression line visually supports a fairly significant relationship between these two variables.

For the 2024 period (Figure 7b), the negative relationship pattern between LST and NDVI was still identified, but with a slightly weaker correlation strength. The correlation coefficient (R) decreased to -0.4588, while the coefficient of determination (R^2) also decreased to 0.2105. This implies that in 2024, only about 21.1% of the NDVI variability can be attributed to changes in LST. The more scattered appearance of the data points compared to the previous year visually confirms the weakening of the relationship between the two variables.

Overall, it can be concluded that there is a statistically significant inverse relationship between Land Surface Temperature and vegetation density in the study area for both years. However, the strength of this relationship is not perfect (R^2 values are far below 1), which implies that LST is not the sole factor controlling NDVI. Other factors such as soil moisture, non-vegetated land cover types, and other biophysical characteristics also contribute, making the LST-NDVI relationship complex and multidimensional (Weng, 2009). Furthermore, the comparison between the years shows temporal variability, where the relationship between LST and NDVI was recorded to be stronger in 2023 than in 2024.

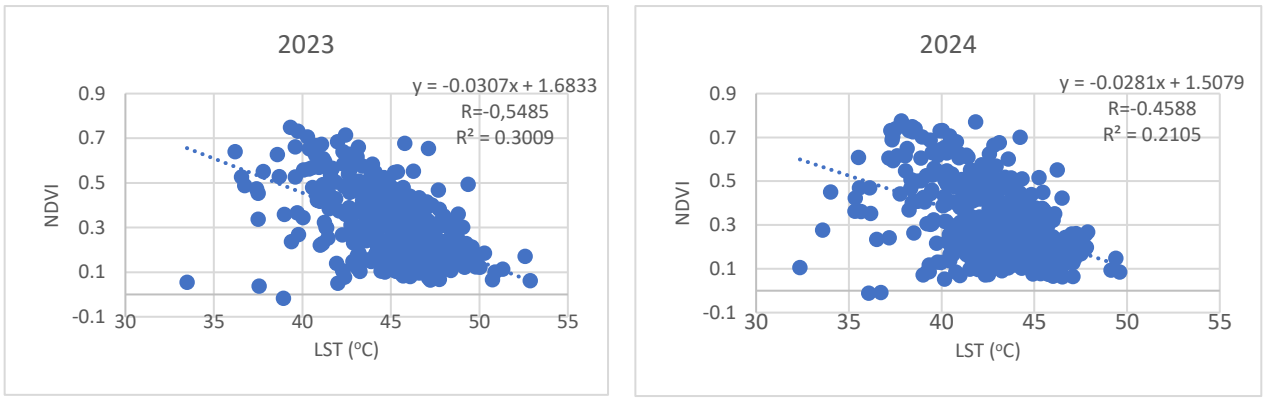

(a) (b)

Figure 7. Scatter plots of LST and NDVI for (a) 2023 and (b) 2024 from combined Landsat 8 and Landsat 9 data.

Quantitative analysis of the relationship between Land Surface Temperature (LST) and the Normalized Difference Vegetation Index (NDVI) for the 2023 and 2024 periods is presented in Tables 4 and 5. The data in both tables consistently show a significant negative correlation between the level of vegetation density and surface temperature. This phenomenon indicates the vital role of vegetation as a thermal regulator in the study area.

Based on the average LST data per vegetation class, a clear pattern was identified where an increase in vegetation density is inversely proportional to a decrease in surface temperature. In 2024 (Table 5), the Dense Vegetation class (NDVI > 0.60) recorded the lowest average LST at 38.74°C. Conversely, the Non-Vegetated class (NDVI < 0.00) showed a much higher average LST of 43.89°C. This progressive decrease in temperature occurs as the vegetation class category increases from sparse to dense.

An analysis of the temperature frequency distribution via histograms for each class reinforces this finding. The histogram for the Non-Vegetated class shows a right-skewed distribution, indicating a concentration of pixels with high LST values. As the vegetation class increases, the peak of the distribution in the histogram systematically shifts to the left, towards lower LST values. For the Dense Vegetation class, the temperature distribution appears more concentrated around a low average value, signifying cooler and more homogeneous thermal conditions.

Furthermore, a comparison of the data between the years shows temporal variability in terms of both thermal conditions and land cover composition. Thermal conditions in 2024 were generally lower than in 2023, as evidenced by the decrease in average LST across all vegetation classes. Additionally, land cover change dynamics were identified, wherein the area of the Dense Vegetation class increased from 36,141 km² in 2023 to 48,542 km² in 2024.

Thus, it can be concluded that vegetation density has a strong influence on the mitigation of land surface temperature in the study area. LST and NDVI data from both observation periods convincingly prove that areas with higher vegetation cover effectively maintain lower surface temperatures. The presence of differences in thermal conditions and class areas between the years also implies the importance of multi-temporal analysis to comprehensively understand the dynamics of the urban environment.

Table 4. Relationship between LST and NDVI according to NDVI Class for the Year 2023.

Classification	Area (km²)	Mean LST (°C)	LST Histogram
Non-Vegetated -1,00 - 0,00	1,117	35,86	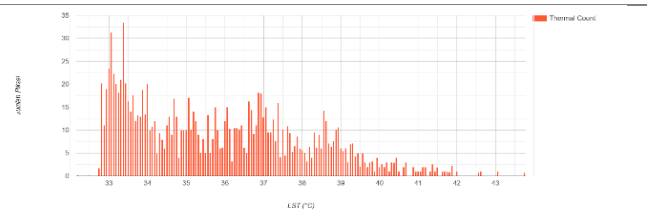
Slightly density 0,00 - 0,30	378,781	46,09	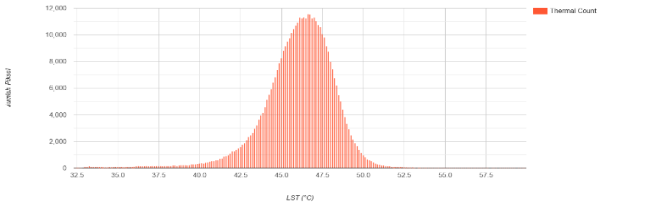
Moderately density 0,30 - 0,60	225,216	43,86	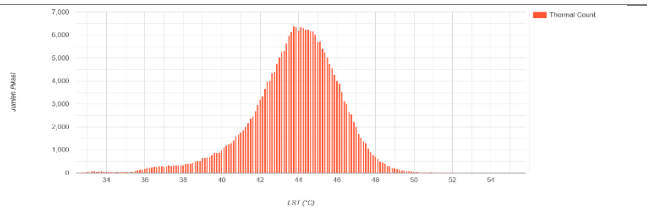
Highly density 0,60 - 1,00	36,141	40,34	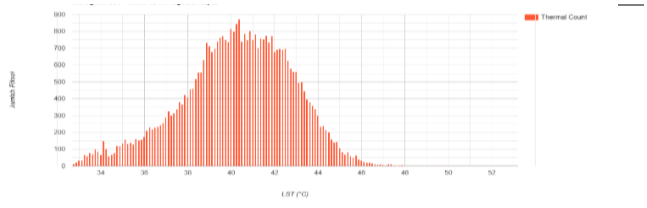

Table 5. Relationship between LST and NDVI according to NDVI Class for the Year 2024.

Classification	Area (km²)	Mean LST (°C)	LST Histogram
Non-Vegetated -1,00 - 0,00	1,193	33,89	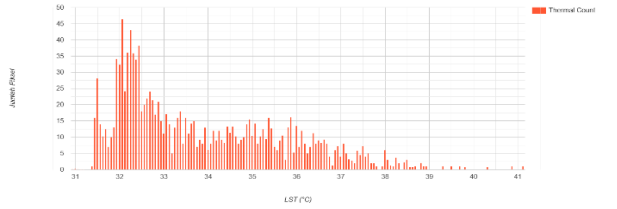
Slightly density 0,00 - 0,30	369,126	43,65	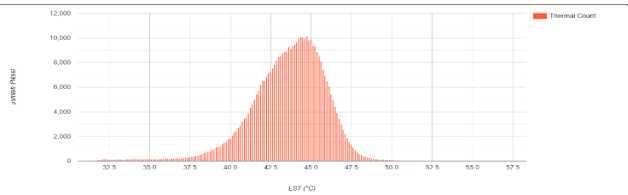
Moderately density 0,30 - 0,60	222,394	41,87	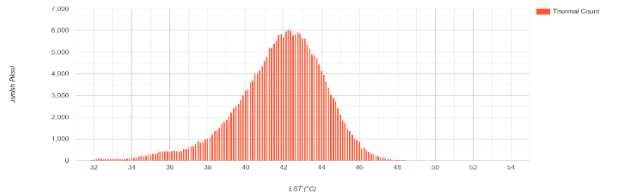
Highly density 0,60 - 1,00	48,542	38,74	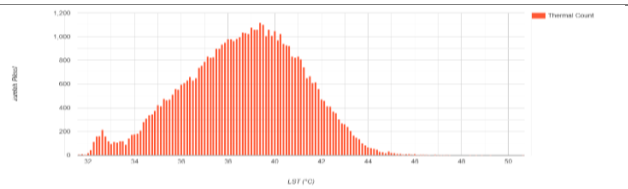

Analysis of the Relationship between LST and NDBI Using Combined Landsat 8 and Landsat 9 Data

To analyze the relationship between surface thermal conditions and the level of urban development, a linear regression analysis was performed between Land Surface Temperature (LST) and the Normalized Difference Built-up Index (NDBI). The quantitative analysis results for the 2023 and 2024 periods, processed from combined Landsat 8 and 9 data, are presented in Figure 8. Overall, the analysis results from both observation periods show a statistically significant positive correlation between LST and NDBI.

In 2023 (Figure 8a), this positive relationship was measured with a correlation coefficient (R) of 0.6966. Meanwhile, in 2024 (Figure 8b), the recorded correlation was 0.6709. The positive correlation values in both years empirically confirm that areas with higher NDBI values reflecting greater built-up density also tend to have higher surface temperatures. Furthermore, the coefficient of determination (R^2) in 2023 was 0.4853, indicating that approximately 48.5% of the variability in NDBI values can be explained by the variability in LST within the study area. The R^2 value for 2024 was slightly lower at 0.4502. The fact that the R^2 values do not approach 1 implies that LST is not the only factor correlated with NDBI.

Based on this analysis, it can be concluded that there is a strong and stable positive relationship between the increase in built-up area density (NDBI) and the increase in Land Surface Temperature (LST) across both observation years.

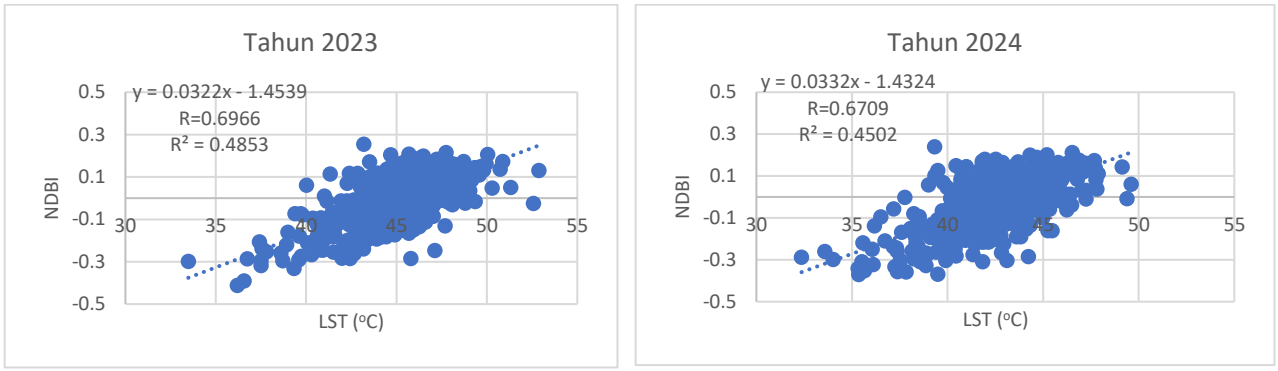

(a) (b)

Figure 8. Scatter plots of LST and NDBI for (a) 2023 and (b) 2024 from combined Landsat 8 and Landsat 9 data.

Tables 6 and 7 present the results of the quantitative analysis on the relationship between Land Surface Temperature (LST) and the density of built-up areas (NDBI) for the 2023 and 2024 periods. The data presented consistently show a positive correlation between an increase in building density and an increase in surface temperature.

An in-depth analysis of both periods shows that the average LST tends to increase with the rise in NDBI class from 'Non-Built-up Area' to 'Dense Built-up'. In 2024 (Table 7), the average LST increased from 41.07°C in the 'Non-Built-up Area' class to 44.73°C in the 'Dense Built-up' class. This temperature increase is caused by the thermal characteristics of urban materials such as concrete and asphalt, which have a higher capacity to absorb and store solar radiation compared to natural surfaces. The temperature frequency distribution presented in the histograms also visually confirms this trend, where the peak of the distribution shifts to the right (towards higher temperatures) as building density increases.

Table 6. Relationship between LST and NDBI according to NDBI Class for the Year 2023.

Classification	Area (km²)	Mean LST (°C)	LST Histogram
Non-Built-up Area -1,0 - 0,0	283,981	43.22	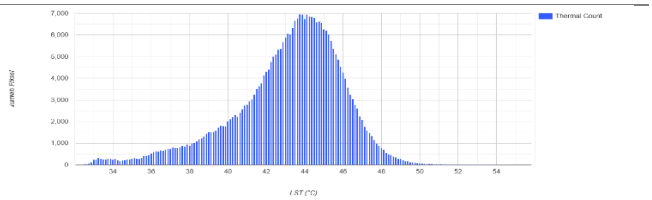
Sparse Built-up 0,0 - 0,1	201,605	45.85	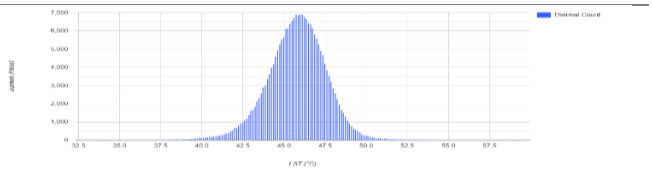
Dense Built-up 0,1 - 0,2	150,564	47.05	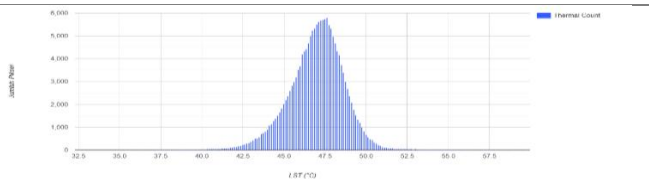
Very Dense Built-up 0,2 - 0,3	5,105	45.43	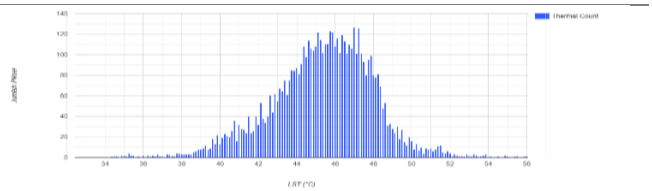

Table 7. Relationship between LST and NDBI according to NDBI Class for the Year 2024.

Classification	Area (km²)	Mean LST (°C)	LST Histogram
Non-Built-up Area -1,0 - 0,0	303,522	41,07	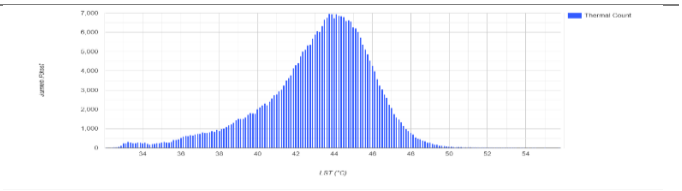
Sparse Built-up 0,0 - 0,1	189,872	43,57	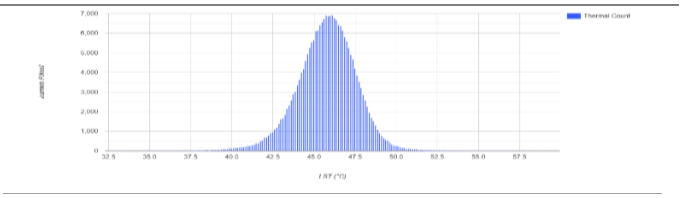
Dense Built-up 0,1 - 0,2	143,461	44,73	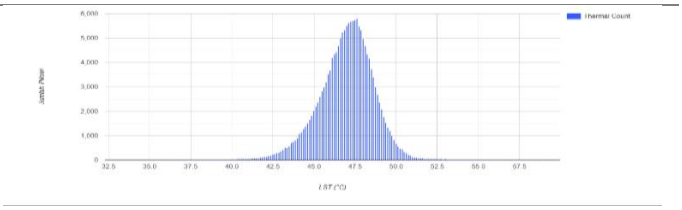
Very Dense Built-up 0,2 - 0,3	4,401	42,98	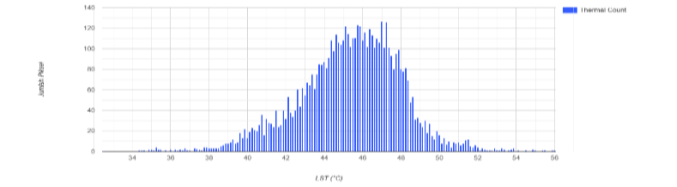

An interesting anomaly was identified in the 'Very Dense Built-up' class (NDBI > 0.2). In both years, this class recorded a slightly lower average LST compared to the 'Dense Built-up' class. This phenomenon indicates that tall, dense buildings can create significant shadowing on the surfaces below, reducing direct exposure to solar radiation. This condition can cause the surface temperature detected by the satellite to be lower compared to areas with the same building density but with lower building heights (Weng, 2009).

A temporal comparison of the data between 2023 and 2024 shows that thermal conditions in 2024 were consistently lower across all NDBI classes. Furthermore, there were changes in the area of each class, indicating dynamics in the urban physical structure during the study period.

It can be concluded that the density of built-up areas is a dominant factor that increases land surface temperature in the study area. However, at the highest density levels, urban geometry factors such as building height and shadowing effects begin to play a role in modulating the surface temperature. This analysis underscores the complexity of the relationship between LST and NDBI.

Analysis of LST, NDVI, and NDBI Using a Combined Landsat 8 and 9 Dataset

Figure 9 presents a visualization of Land Surface Temperature (LST) data in the study area for the years 2023 (a) and 2024 (b), along with frequency distribution histograms for each year, a map of the LST difference between the two years (c), and a histogram of the difference values (d). This analysis aims to identify the spatial distribution patterns of LST and to analyze its distributional characteristics and temporal changes.

The spatial LST maps in Figures 9a and 9b consistently show a similar temperature distribution pattern across both observation years. Areas with the highest surface temperatures (displayed in red and orange) are concentrated in the northern coastal region, the city center, and dense industrial areas, which include North Jakarta, Central Jakarta, and parts of West and East Jakarta. Conversely, areas with relatively lower temperatures (yellow and green) are predominantly found in the southern region (South Jakarta), which

historically has more vegetation cover and green open spaces. Year-to-year changes in LST can be influenced by many factors, including land cover change, weather conditions at the time of image acquisition, and seasonal cycles.

The histograms for both years show an LST distribution that is generally normal but slightly right-skewed (positive skew), with the frequency peak occurring around 40-45°C. This distribution shape implies that a majority of the study area has high surface temperatures, which is characteristic of a dense urban environment. A comparison between the two years reveals slight differences in the recorded maximum temperature ranges, indicating the presence of annual thermal variability.

The temporal change analysis presented in the LST difference map (Figure 9c) shows locations that experienced significant temperature changes. Areas marked in green represent cooling (2024 temperatures were lower than 2023), while red indicates warming. This map allows for the identification of specific areas that underwent an increase or decrease in surface temperature, which can be an indication of significant environmental changes, such as the conversion of green space to built-up areas or vice versa. The spatial extent of high surface temperature zones is continually expanding, concurrent with the conversion of land into built-up areas (Danniswari et al., 2020). This transformation process leads to an increase in surface temperature, which in turn contributes to a wider distribution of high thermal zones across the region. Figure 9d provides a quantitative overview of this change. The shape of the histogram shows a frequency distribution centered with a sharp peak to the left. This distribution shape implies that the majority of the study area experienced a decrease in surface temperature, where 2023 was warmer than 2024.

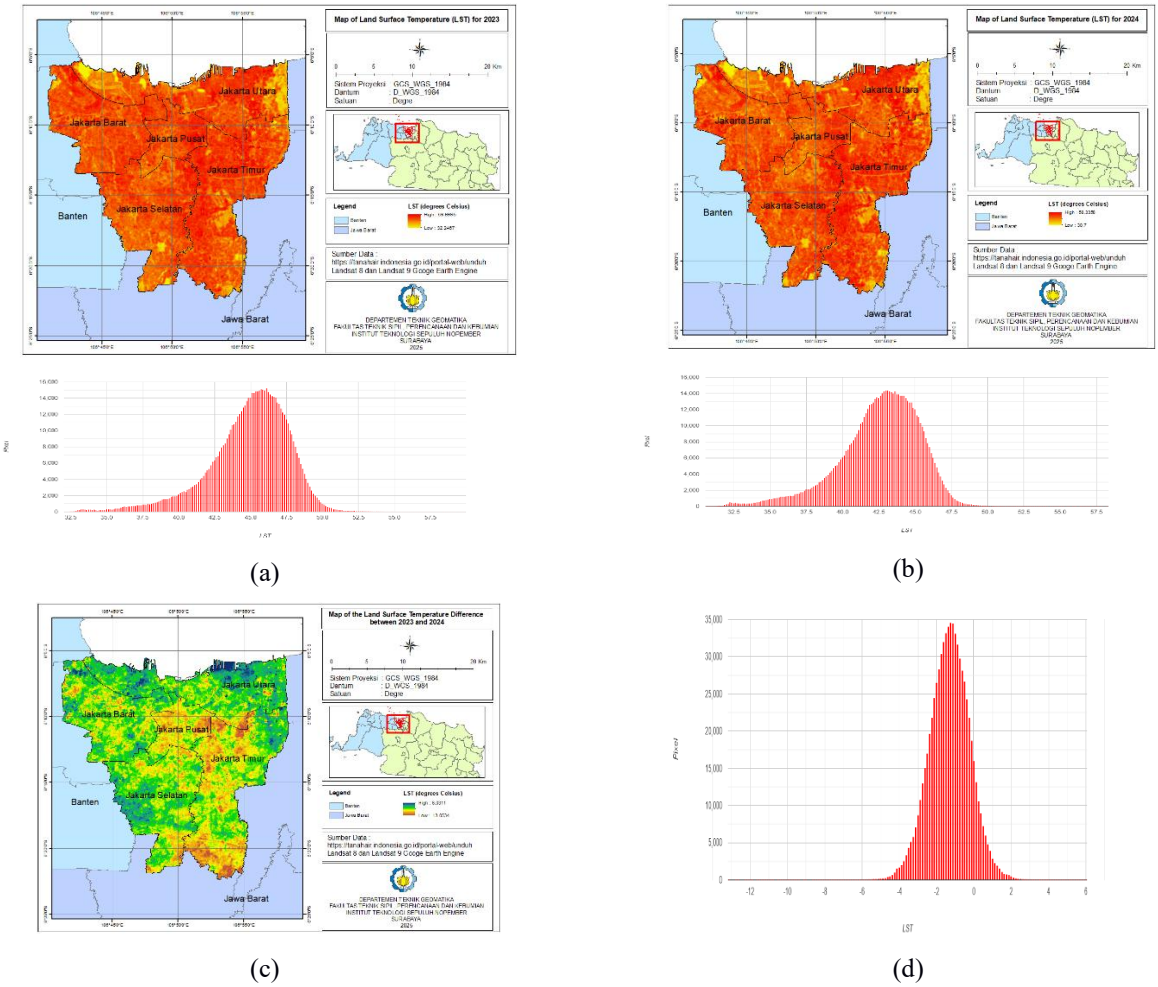

Figure 9. LST maps and histograms for (a) 2023 and (b) 2024, along with (c) the LST difference map for 2024–2023 and (d) the histogram of the LST difference, derived from combined Landsat 8 and Landsat 9 data

Figure 10 presents a visualization of Normalized Difference Vegetation Index (NDVI) data in the study area for 2023 (a) and 2024 (b), along with frequency distribution histograms for each year. It also specifically maps the difference in NDVI values between 2024 and 2023 (c), while (d) displays the histogram of the distribution of these difference values. This analysis aims to identify the spatial distribution patterns of vegetation density and to understand its general distributional characteristics.

The spatial NDVI map in Figure 10a shows the distribution of NDVI values in the Jakarta region in 2023. The color scale on the map indicates the level of vegetation greenness, where dark green represents areas with very high and healthy vegetation density, while yellow or light green shows sparser vegetation or areas with non-vegetated cover. It is observed that most of the Jakarta region is dominated by green colors, indicating the presence of vegetation, albeit with varying levels of density. Areas with high NDVI (dark green) tend to be concentrated in green open spaces, city parks, and suburban areas that still have open land. The 2024 NDVI map (Figure 10b) shows a similar distribution pattern to 2023. However, fluctuations in NDVI values can occur due to seasonal changes, rainfall, or development activities that reduce vegetation cover. This map reveals several micro-level changes at various locations, which may indicate environmental changes within the one-year period.

The histograms for both years show a right-skewed (positive skew) distribution of NDVI values, with the frequency peak occurring in the 0.2 to 0.4 range. This distribution shape implies that most of the study area is covered by vegetation of low to moderate density. The distribution's tail extending towards higher NDVI values indicates the presence of areas with denser vegetation cover, although their extent is not dominant.

The NDVI difference map (Figure 10c) shows the dynamics of vegetation change, which vary spatially. Areas marked in green represent an increase in NDVI values, indicating an increase in greenness or vegetation density in 2024 compared to 2023. Conversely, areas in blue or pale yellow show minimal change or a slight decrease in greenness. The histogram in Figure 10d provides a quantitative overview of the distribution of the overall NDVI difference. The shape of the histogram shows a very sharp and narrow peak centered on an NDVI range close to zero. This indicates that the majority of pixels in the study area did not experience significant changes in greenness between 2023 and 2024.

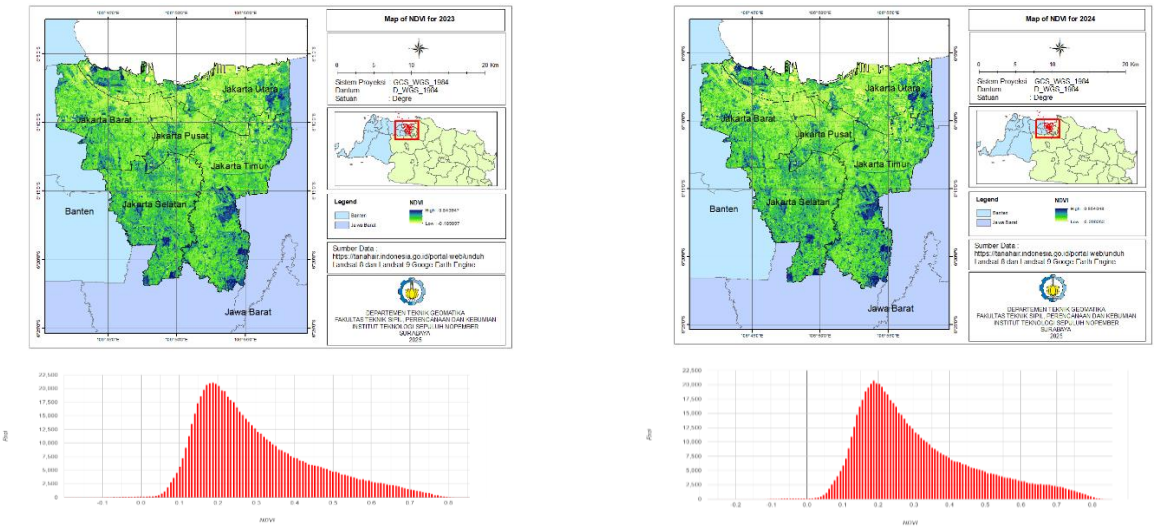

(a) (b)

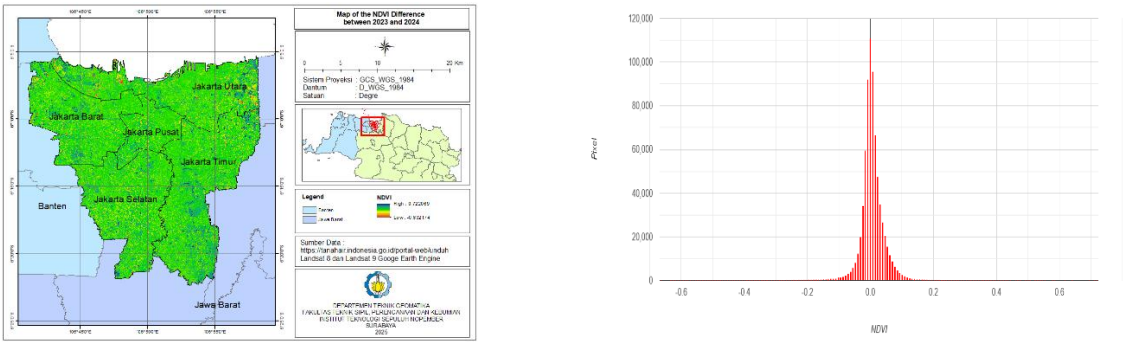

(c) (d)

Figure 10. NDVI maps and histograms for (a) 2023 and (b) 2024, along with (c) the NDVI difference map for 2024–2023 and (d) the histogram of the NDVI difference, derived from combined Landsat 8 and Landsat 9 data

High-resolution satellite imagery from Google Earth was used to corroborate the land cover conditions before and after the observed changes. The study area in 2023 (Figures 11b) was predominantly comprised of a water body and some open land, both of which are land cover types that naturally produce low NDVI values. This is because water absorbs a majority of near-infrared (NIR) radiation, while open land is characterized by an absence of photosynthetic activity. In contrast, the imagery acquired in 2024 (Figures 11c) shows a fundamental conversion to vegetative cover. This transformation, presumably caused by land reclamation activities, resulted in the growth of pioneer vegetation like grass, which possesses high NIR reflectance. Consequently, the measured quantitative increase in the NDVI is directly attributable to the conversion of non-vegetated land cover to vegetated land cover.

(a) (b) (c)

Figure 11. (a) NDVI difference map for 2024–2023 (b) Google Earth satellite imagery in 2023 (c) Google Earth satellite imagery in 2024

Figure 12 presents the spatial analysis and frequency distribution of the Normalized Difference Built-up Index (NDBI) in the study area. Figures 12a and 12b specifically map the NDBI conditions for 2023 and 2024, respectively; Figure 12c maps the difference in NDBI values between the two years, while Figure 12d displays the histogram of the distribution of these difference values. This analysis aims to identify changes in built-up areas spatially and to understand the general characteristics of land cover in the study area.

The spatial NDBI map in Figure 12a shows the NDBI distribution in the DKI Jakarta region in 2023. The color scale on the map indicates the level of building density, where red shows very high building density and green shows areas with low building density or vegetation cover. Most areas in Central Jakarta, West Jakarta, and North Jakarta, especially in the urban core areas, are dominated by high NDBI values (red), which reflects the high building density. This is in line with Jakarta's characteristics as a megapolitan with rapid infrastructure development. Figure 12b shows a similar distribution pattern to 2023. However, with ongoing development and land cover changes, several micro-level changes are visible at various locations. An increase in the intensity of the red color in some areas indicates an increase in building density, either through the construction of new buildings or the conversion of non-built-up land into built-up areas.

The histograms accompanying both maps show the frequency distribution of NDBI values throughout the study area. In both 2023 and 2024, the histograms show a right-skewed distribution, indicating that most pixels have low NDBI values. This could be due to the presence of non-built-up areas such as water bodies (Jakarta Bay), green open spaces, and suburban areas that still have vegetation cover.

The NDBI difference map (Figure 12c) shows that there were changes in building density that varied spatially. Areas marked in green represent an increase in NDBI values, which indicates an increase in building density or new development in 2024 compared to 2023. Conversely, areas in blue or pale yellow show minimal change or a slight decrease in building density. This map allows for the identification of specific locations that have undergone intensive urbanization within a one-year period, which can be targets for spatial planning policy interventions. The shape of the histogram in Figure 12d shows a very sharp and narrow peak centered on an NDBI range close to zero. This indicates that the majority of pixels in the study area did not experience significant changes in building density between 2023 and 2024.

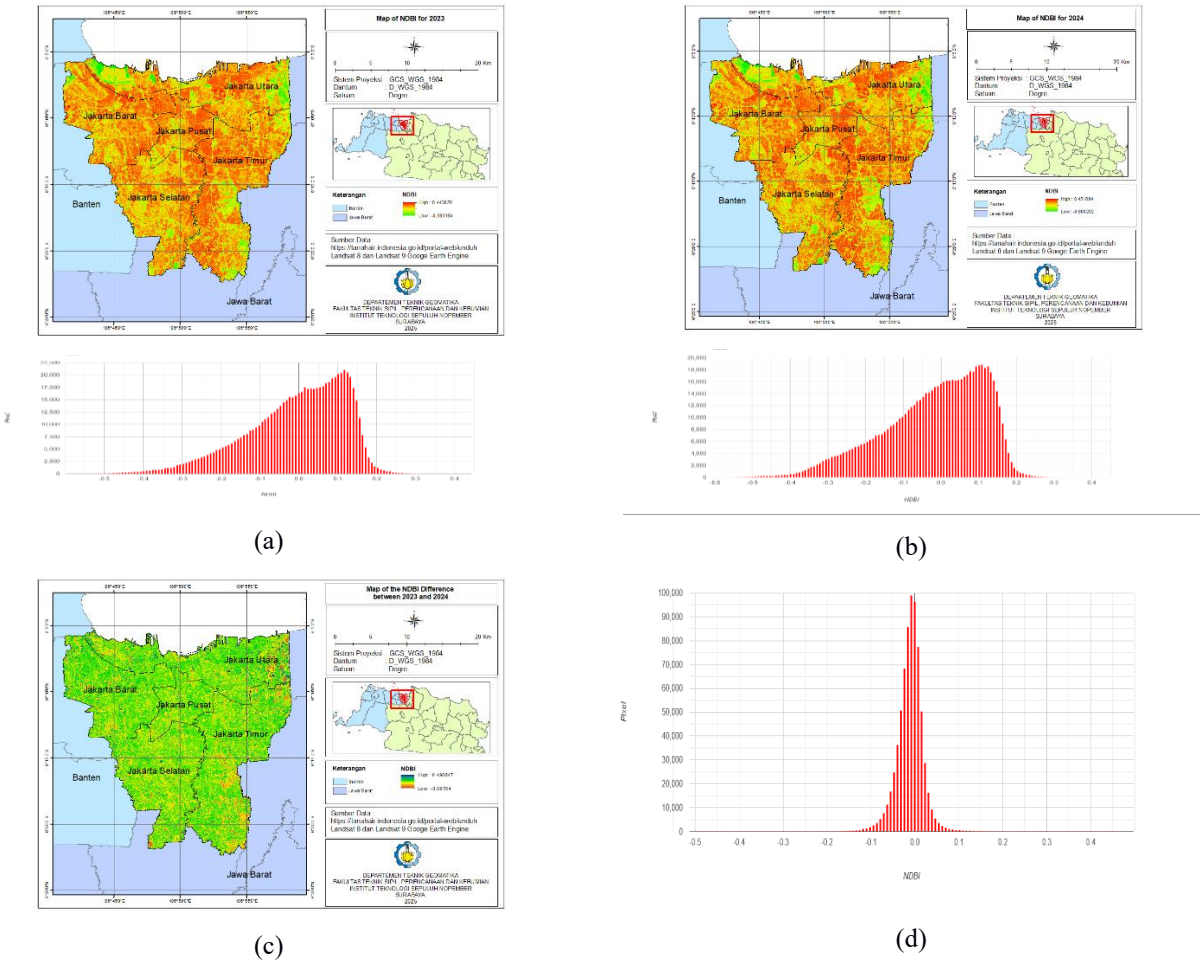

Figure 12. NDBI maps and histograms for (a) 2023 and (b) 2024, along with (c) the NDBI difference map for 2024–2023 and (d) the histogram of the NDBI difference, derived from combined Landsat 8 and Landsat 9 data

A diachronic analysis of high resolution Google Earth imagery was conducted to validate the anomalous increase in NDBI. In 2023 (Figure 13b), the site was a land cover mosaic composed of green open space (dense vegetation) and a small fraction of built-up areas. Biophysically, the high proportion of vegetation caused an attenuation (weakening) of the NDBI value, as the strong Near Infrared (NIR) reflectance from the canopy masked the spectral response of existing impermeable surfaces. However, a massive land cover transformation occurred in 2024 (Figure 13c). Land clearing activities replaced most of the vegetation with new infrastructure development. This newly formed surface, dominated by construction materials, inherently possesses high NIR absorption and high Short Wave Infrared (SWIR) reflectance properties. This mechanism the shift in spectral

response from NIR dominance (vegetation) to SWIR dominance (buildings) quantitatively explains the spike in NDBI values at the location.

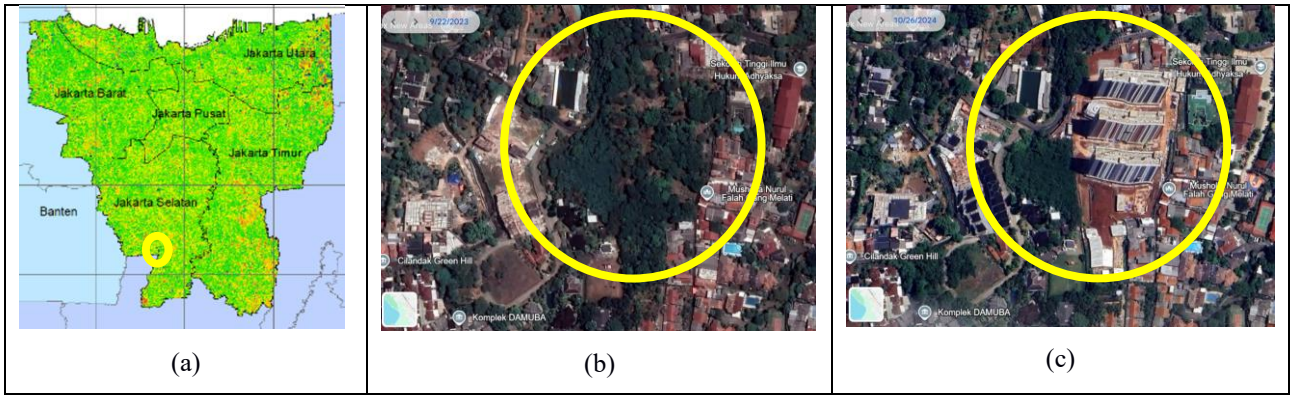

(a) (b) (c)

Figure 13. (a) NDBI difference map for 2024–2023 (b) Google Earth satellite imagery in 2023 (c) Google Earth satellite imagery in 2024

Conclusions

Overall, the research results show that the Land Surface Temperature (LST), Normalized Difference Vegetation Index (NDVI), and Normalized Difference Built-up Index (NDBI) data produced by the Landsat 8 and Landsat 9 satellites exhibit a very high degree of consistency and agreement ($R > 0.86$ for LST; $R > 0.97$ for NDVI and NDBI). This proves that the data from both missions are reliable and can be combined, thereby enabling multi-temporal analysis with a higher temporal resolution.

There are significant and opposing correlations between surface thermal conditions and land cover types of vegetation and built-up areas. A strong negative correlation was found between LST and NDVI, where an increase in vegetation density effectively lowers the land surface temperature. Conversely, there is a strong positive correlation between LST and NDBI, which proves that an increase in building density is a dominant factor triggering a rise in surface temperature.

The temporal analysis between 2023 and 2024 indicates dynamics in both thermal conditions and land cover composition. In general, thermal conditions in 2024 were lower than in 2023 across all land cover classes. Although massive land cover change was not detected, the analysis of the NDVI and NDBI differences indicates the presence of localized micro-changes, such as increases in vegetation and building density at specific points.

Urban geometry at the highest levels of building density shows a complex influence on LST. An anomaly was identified where the 'Very Dense Built-up' class has a slightly lower average temperature than the 'Dense Built-up' class. This phenomenon is presumably caused by the shading effect of tall buildings, which reduces the surface's exposure to solar radiation, affirming that in addition to land cover composition, the three-dimensional structure of the city also plays a role in modulating the microclimate.

Acknowledgment

The authors gratefully acknowledge the financial support for this research from the Center for Human Resources Development (PPSDM) of the Indonesian Agency for Meteorology, Climatology, and Geophysics (BMKG). Gratitude is also extended to the BMKG for providing the in-situ air temperature data. We would also like to thank the U.S. Geological Survey (USGS) for providing the Landsat 8 and Landsat 9 data used in this study.

References

Danniswari, D., Honjo, T., & Furuya, K. (2020). Land Cover Change Impacts on Land Surface Temperature in Jakarta and Its Satellite Cities. *IOP Conference Series: Earth and Environmental Science*, *501*(1). https://doi.org/10.1088/1755-1315/501/1/012031

Fatkhuroyan, & TrinahWati. (2018). Accuracy Assessment of Global Satellite Mapping of Precipitation (GSMaP) Product over Indonesian Maritime Continent. *IOP Conference Series: Earth and Environmental Science*, *187*(1). https://doi.org/10.1088/1755-1315/187/1/012060

Gorelick, N., Hancher, M., Dixon, M., Ilyushchenko, S., Thau, D., & Moore, R. (2017). Google Earth Engine: Planetary-scale geospatial analysis for everyone. *Remote Sensing of Environment*, *202*, 18–27. https://doi.org/10.1016/j.rse.2017.06.031

Gunawan, R. A. R., Hadibasyir, H. Z., & Arijuddin, B. I. (2023). Analysis of the Impact of Residential Land Development on LST in Semarang City. *Proceedings of the International Conference of Geography and Disaster Management (ICGDM 2022)*, 421–435. https://doi.org/10.2991/978-2-38476-066-4_27

Gusmiarti, N., Prasetyo, Y., & Bashit, N. (2022). Analisis Korelasi Land Surface Temperature (LST) dengan Penerapan Pembatasan Kegiatan Masyarakat (PKM) (Studi Kasus : Kawasan Sentra Pengasapan Ikan, Bandarharjo, Semarang). *Elipsoida : Jurnal Geodesi Dan Geomatika*, *5*, 61–68. https://doi.org/10.14710/elipsoida.2022.16741

Hardianto, A., Dewi, P. U., Feriansyah, T., Sari, N. F. S., & Rifiana, N. S. (2021). Pemanfaatan Citra Landsat 8 Dalam Mengidentifikasi Nilai Indeks Kerapatan Vegetasi (NDVI) Tahun 2013 dan 2019 (Area Studi: Kota Bandar Lampung). *Jurnal Geosains Dan Remote Sensing*, *2*(1), 8–15. https://doi.org/10.23960/jgrs.2021.v2i1.38

Jannah, G., & Bioresita, F. (2023). Pemantauan Land Surface Temperature (LST) dan Kaitannya dengan Tutupan Lahan (Studi Kasus: Kota Surabaya Tahun 2014-2022). *Jurnal Teknik ITS*, *12*. https://doi.org/10.12962/j23373539.v12i2.122579

Jiménez-Muñoz, J. C., Sobrino, J. A., Skoković, D., Mattar, C., & Cristóbal, J. (2014). Land Surface Temperature Retrieval Methods From Landsat-8 Thermal Infrared Sensor Data. *IEEE Geoscience and Remote Sensing Letters*, *11*(10), 1840–1843. https://doi.org/10.1109/LGRS.2014.2312032

Kumar, L., & Mutanga, O. (2018). Google Earth Engine Applications Since Inception: Usage, Trends, and Potential. *Remote Sensing*, *10*, 1509. https://doi.org/10.3390/rs10101509

Laksono, A., Saputri, A. A., Pratiwi, C. I. B., Arkan, M. Z., & Putri, R. F. (2020). Vegetation covers change and its impact on Barchan Dune morphology in Parangtritis Coast, Indonesia. *E3S Web of Conferences*, *200*. https://doi.org/10.1051/e3sconf/202020002026

Li, Z.-L., Tang, B., Wu, H., Yan, G., Wan, Z., Trigo, I., & Sobrino, J. (2013). Satellite-Derived Land Surface Temperature: Current Status and Perspectives. *Remote Sensing of Environment*, *131*, 14–37. https://doi.org/10.1016/j.rse.2012.12.008

Masek, J., Wulder, M., Markham, B., McCorkel, J., Crawford, C., Storey, J., & Jenstrom, D. (2020). Landsat 9: Empowering open science and applications through continuity. *Remote Sensing of Environment*, *248*, 111968. https://doi.org/10.1016/j.rse.2020.111968

Mashudi, M., & Faisol, A. (2022). Estimasi Suhu Udara Di Kabupaten Manokwari Melalui Pemanfaatan Citra Satelit Landsat 8. *Jurnal Meteorologi Dan Geofisika*, *23*(1), 52. https://doi.org/10.31172/jmg.v23i1.753

Meng, X., & Cheng, J. (2018). Evaluating Eight Global Reanalysis Products for Atmospheric Correction of Thermal Infrared Sensor—Application to Landsat 8 TIRS10 Data. *Remote Sensing*, *10*, 474. https://doi.org/10.3390/rs10030474

Mustafa, P. S. (2023). Tinjauan Literatur Analisis Uji R Berganda dan Uji Lanjut dalam Statistik Inferensial pada Penelitian Pendidikan Jasmani. *Jurnal Ilmiah Wahana Pendidikan*, *2023*(5), 571–593. https://doi.org/10.5281/zenodo.7758162

Prayogo, L. (2021). Platform Google Earth Engine Untuk Pemetaan Suhu Permukaan Daratan Dari Data Series Modis. *DOUBLECLICK Journal of Computer and Information Technology*, *5*, 25–31. https://doi.org/10.25273/doubleclick.v5i1.8604

Putu Aryastana, I Gede Yogi Adnyana Puspita Riana, Ilona Dwiyeni Nahak, I Wayan Wartana, & Ida Bagus Made Yatana. (2023). Analisis indeks vegetasi pada citra Landsat 8 untuk penentuan perubahan tutupan lahan di Kabupaten Badung, Provinsi Bali. *PADURAKSA: Jurnal Teknik Sipil Universitas Warmadewa*, *12*(2), 127–136. https://doi.org/10.22225/pd.12.2.6370.127-136

Sampelan, D., Baihaqi, A., & Jaelani, L. M. (2024). Analyzing the Impact of Mandalika Special Economic Zone (SEZ) Development on Land Surface Temperature (LST) Using Landsat 8 Satellite Imagery. *2024 IEEE Asia-Pacific Conference on Geoscience, Electronics and Remote Sensing Technology (AGERS)*, 16–23. https://doi.org/10.1109/AGERS65212.2024.10932919

Tamiminia, H., Salehi, B., Mahdianpari, M., Quackenbush, L., Adeli, S., & Brisco, B. (2020). Google Earth Engine for geo-big data applications: A meta-analysis and systematic review. *ISPRS Journal of Photogrammetry and Remote Sensing*, *164*, 152–170. https://doi.org/10.1016/J.ISPRSJPRS.2020.04.001

Tang, B., Shao, K., Li, Z.-L., Wu, H., & Tang, R. (2015). An improved NDVI-based threshold method for estimating land surface emissivity using MODIS satellite data. *International Journal of Remote Sensing*, *36*, 1–15. https://doi.org/10.1080/01431161.2015.1040132

USGS. (2021). *Landsat 9 Data Users Handbook*.

USGS. (2024). *Landsat 8-9 Collection 2 (C2) Level 2 Science Product (L2SP) Guide*.

USGS. (2025, September 5). *How do I use a scale factor with Landsat Level-2 science products?* https://www.usgs.gov/faqs/how-do-i-use-a-scale-factor-landsat-level-2-science-products

Weng, Q. (2009). Thermal infrared remote sensing for urban climate and environmental studies: Methods, applications, and trends. In *ISPRS Journal of Photogrammetry and Remote Sensing* (Vol. 64, Issue 4, pp. 335–344). https://doi.org/10.1016/j.isprsjprs.2009.03.007

Weng, Q., Lu, D., & Schubring, J. (2004). Estimation of land surface temperature-vegetation abundance relationship for urban heat island studies. *Remote Sensing of Environment*, *89*, 467–483. https://doi.org/10.1016/j.rse.2003.11.005

Xu, H., Ren, M., & Lin, M. (2024). Cross-comparison of Landsat-8 and Landsat-9 data: a three-level approach based on underfly images. *GIScience and Remote Sensing*, *61*(1). https://doi.org/10.1080/15481603.2024.2318071

Zha, Y., Gao, J., & Ni, S. (2003). Use of normalized difference built-up index in automatically mapping urban areas from TM imagery. *International Journal of Remote Sensing - INT J REMOTE SENS*, *24*, 583–594. https://doi.org/10.1080/01431160304987